

## Structure-activity relationships of autotaxin inhibition

Lauren E. Ragle, Daniel L. Baker and Abby L. Parrill\*

Department of Chemistry, University of Memphis, 3744 Walker Ave, Memphis, TN 38152, USA.

### ABSTRACT

Autotaxin (ATX) is a ubiquitous ectoenzyme that hydrolyzes lysophosphatidylcholine to form the bioactive lipid mediator lysophosphatidic acid (LPA). LPA activates specific G-protein-coupled receptors to elicit downstream effects leading to cellular motility, survival, and invasion. Through these downstream effects, autotaxin is involved in many human disorders including cancer, heart disease, chronic pain, asthma, and other inflammatory diseases. Inhibition of autotaxin activity is therefore a therapeutically attractive goal. This review will summarize insights into the inhibition of ATX gained across multiple structure-activity relationship (SAR) studies. Initial ATX inhibitors included metal chelators such as L-histidine and analogs. Subsequently, the bioactive lipids LPA and sphingosine-1-phosphate were identified as ATX feedback inhibitors, which lead to extensive SAR studies on phospholipid analogs. Subsequently, computational and experimental SAR studies have allowed for the discovery of small, non-lipid ATX inhibitors that, in many cases, avoid G-protein-coupled receptor-mediated off-target effects. Crystal structures of ATX inhibitor complexes have been reported starting from 2011, confirming earlier enzyme kinetic studies that suggested multiple inhibitor binding sites. These structures revealed a unique allosteric hydrophobic pocket within the ATX catalytic domain. Further exploration of this hydrophobic pocket, both computationally and experimentally, has been undertaken to develop additional ATX inhibitors that take advantage of hydrophobic interactions.

**KEYWORDS:** autotaxin, structure-activity relationship, inhibitors

### ABBREVIATIONS

ATX	: autotaxin
bis-pNPP	: bis( <i>para</i> -nitrophenyl) phosphate
EDTA	: ethylenediaminetetraacetic acid
FRET	: fluorescence resonance energy transfer
GPCR	: G-protein coupled receptor
hERG	: human Ether-a-go-go-Related Gene
LC-MS/MS	: liquid chromatography-tandem mass spectrometry
LogP	: log of the octanol/water partition coefficient
LPA	: lysophosphatidic acid
LPAR	: lysophosphatidic acid receptor
LPC	: lysophosphatidylcholine
lysoPLD	: lysophospholipase-D
MOE	: Molecular Operating Environment
NPP	: nucleotide pyrophosphatase phosphodiesterase
PDB	: Protein Data Bank
pNP-TMP	: thymidine 5'-4-nitrophenyl phosphate
SAR	: structure-activity relationship
S1P	: sphingosine-1-phosphate
TUDCA	: tauroursodeoxycholic acid

### INTRODUCTION

Autotaxin (ATX, also known as NPP2) was confirmed in 2002 by two independent research groups, to be the protein responsible for a long studied plasma lysophospholipase-D (lysoPLD) activity and by extension the source of serum lysophosphatidic acid [1, 2]. This realization served as a convergence

---

\*Corresponding author: aparrill@memphis.edu

point for two previously disparate fields of study. Historically, ATX research had been divided into investigations of enzymatic function in plasma (*via* lysoPLD activity) and investigations using purified enzyme (ATX), mostly from melanoma conditioned culture media. Studies on enzymatic function of plasma lysoPLD were initiated in the 1980s to understand the formation of bioactive lipids in plasma and serum [3, 4]. Tokumura *et al.* connected plasma lysoPLD activity to the generation of lysophosphatidic acid *via* hydrolysis of lysophosphatidylcholine (Figure 1) [4]. This work showed that addition of  $\text{Co}^{2+}$  or  $\text{Zn}^{2+}$  was beneficial to plasma lysoPLD activity [5]. When ATX was later crystallized in 2011, the importance of divalent metals was confirmed as two  $\text{Zn}^{2+}$  ions were present in the active site [6, 7]. Investigations into purified ATX enzyme began in 1992 when Stracke *et al.* purified an autocrine motility factor from melanoma cells. They identified this unique glycoprotein as ATX [8]. This work also connected ATX to pertussis toxin-sensitive G-proteins, which suggested specific downstream G-protein-coupled receptor (GPCR) activation. ATX was also determined to have both pyrophosphatase and phosphodiesterase activities including nucleotide hydrolysis through a common catalytic site [9]. Once ATX was shown to be responsible for plasma lysoPLD activity and thereby the primary source of plasma LPA (Figure 1), the relationship of ATX to pertussis-toxin sensitive GPCRs seen by Stracke *et al.* was validated [8]. Jansen *et al.* elucidated the mechanism by which ATX is released from cells by a process of proteolytic maturation [10].

ATX is one member of a larger pyrophosphatase/phosphodiesterase family of ectoenzymes. ATX possesses phosphodiesterase activity toward phospholipids as shown in figure 1 and pyrophosphatase activity against nucleotide di- and tri-phosphates [1, 2, 9]. This dual specificity

is unique to known NPP family members as NPP1, NPP3, and NPP4 preferentially hydrolyze nucleotides [11-13]. In contrast, NPP6 and NPP7 both utilize lipid substrates [14]. To date the natural substrate of NPP5 remains unknown. Most biological effects from ATX activity have been shown to be mediated by the action of its major product, LPA, on specific GPCRs [15-17].

During normal homeostasis, ATX plays important roles in wound healing and *in utero* blood vessel development [18-21]. However, when ATX expression/activity becomes dysregulated, cellular proliferation and migration can lead to several disease states including cancer and other inflammatory diseases [8, 22]. Several different lines of evidence support a role for ATX in cancer. First, as previously stated, ATX was identified as the enzyme responsible for cell motility in melanoma A2058 cells [8]. Second, ATX was found to increase cellular invasion through autocrine signaling pathways in both glioblastoma multiforme and acute myeloid leukemia [23-25]. Third, ATX expression was shown to be connected with increased levels of inflammatory cytokines in both breast and thyroid cancer [17, 26, 27]. Fourth, ATX expression is elevated in endothelial cells lining tumor vessels of renal cell carcinoma [28].

The role of LPA and ATX has been studied in chemotherapeutic resistance, as well. ATX leads to acquired resistance to a common chemotherapeutic, sunitinib, which is antagonized by treatment with an  $\text{LPA}_1$  receptor antagonist [28]. ATX-produced LPA has also been linked to chemotherapeutic resistance in ovarian cancer cells treated with carboplatin [29] and breast cancer cells treated with Taxol [30]. Inhibition of ATX has been shown to sensitize cells to chemotherapy-induced apoptosis, which delays or avoids resistance pathways [29]. Therefore, ATX inhibition is a therapeutic target for chemotherapeutic resistance.

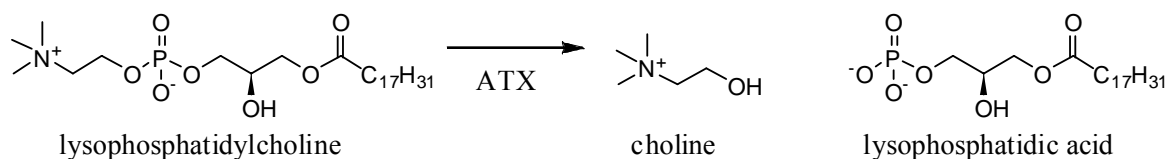


**Figure 1.** Generation of lysophosphatidic acid (LPA) by ATX-catalyzed hydrolysis of lysophosphatidylcholine (LPC).

ATX has also been linked with other human health issues, including both liver fibrosis and pulmonary idiopathic fibrosis [31, 32]. Additionally, ATX has been connected to coronary disease due to a marked increase in plasma LPA [33]. ATX-catalyzed production of LPA has also been implicated in models of chronic neuropathic pain and allergic asthma [34-36]. Increased ATX expression has also been found in the frontal cortex of Alzheimer-type dementia patients and is theorized to be a potential risk factor marker and biological target for advanced Alzheimer's disease [37]. ATX secreted by adipose tissue produces LPA, resulting in negative feedback which has been linked to obesity and obesity-related dysregulation of glucose homeostasis [38]. ATX inhibition is thus also a therapeutic target for inflammatory diseases.

#### **Assays to determine autotaxin activity/inhibition**

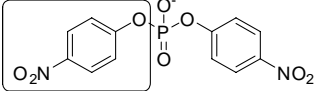
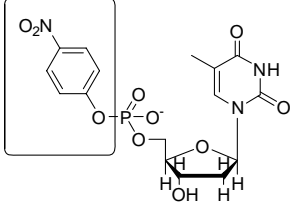
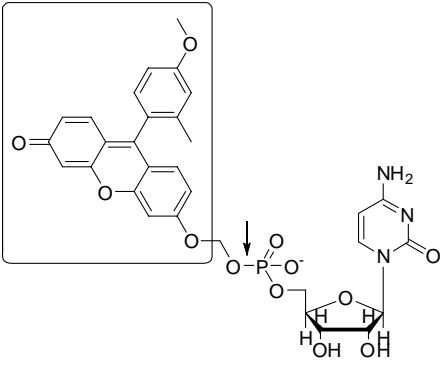
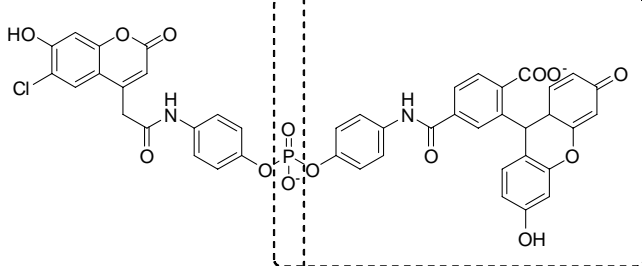
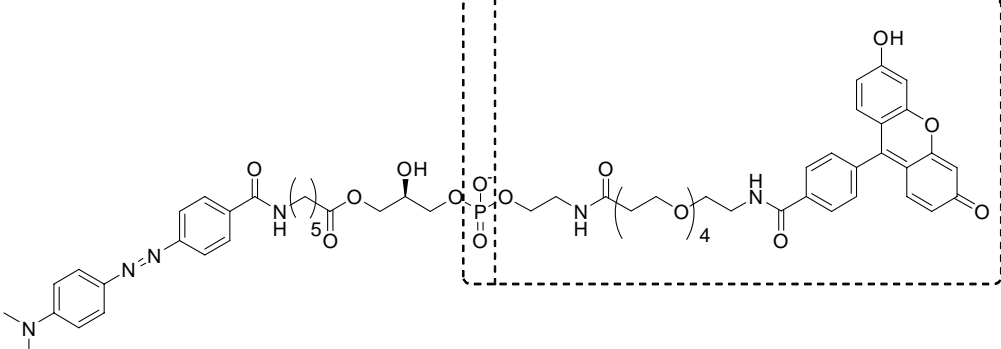
Upon hydrolysis by ATX, LPC releases both choline and LPA (Figure 1), both of which can be detected in medium and high-throughput biochemical assays. These assays are commonly used to determine ATX activity and to screen candidate inhibitors. These assays make use of either natural or unnatural substrates. Natural substrates, such as LPC, including those with varying acyl chain lengths and degrees of unsaturation have been incorporated into several methods [2, 39-41]. Radiolabeled  $^{14}\text{C}$ -LPC is also a direct method, but it is not suitable for high-throughput screening due to the necessity of purifying the product (LPA) from the starting material (LPC) before the activity can be determined [2, 42]. Choline release can be detected by enzyme-catalyzed oxidation of choline to betaine by choline oxidase, releasing hydrogen peroxide, which can react with a variety of reagents including horseradish peroxidase to generate a detectable product, but due to addition of other enzymes, there is a high likelihood of assay interference [43-48]. LPA can be detected directly and in a highly-sensitive manner with liquid chromatography-tandem mass spectrometry (LC-MS/MS) methods [6, 49]. Several unnatural substrates have also been used to measure ATX inhibition (Table 1). These substrates are used in either absorbance- or FRET-based fluorescence

assays. Both bis-4-nitrophenylphosphate and thymidine 5'-4-nitrophenyl phosphate (pNP-TMP) release 4-nitrophenolate, which absorbs at 405 nm and can be readily detected in a high-throughput manner [1, 42, 50]. Another fluorescence-based probe, TG-mTMP, was designed by Kawaguchi *et al.* to improve fluorescence quantum yield and to take advantage of nucleotide recognition by ATX (Table 1) [51]. Competitive ATX inhibitors may be allosteric inhibitors or non-inhibitors of smaller substrates such as pNP-TMP and TG-mTMP. Longer, FRET-based substrates such as CPF4 and FS-3 (Table 1) can be used in high-throughput assays whereupon hydrolysis of the phosphodiester bond by ATX will release a fluorescent product [52, 53].

These longer substrates may be more suitable for determining inhibition by molecules that bind outside of the active site, in addition to those that are within the active site. Because of the differences in binding mechanisms, more than one substrate is typically used to identify new ATX inhibitors. For instance, hydrolysis of smaller substrates may not necessarily be inhibited by the presence of compounds binding outside of the central region of the active site. Therefore, a combination of both longer and smaller substrates should be used to identify new ATX inhibitors.

Because more than one assay method is typically used to assess ATX activity, comparing ATX inhibitors is challenging. Differences in assays (substrate identity, and enzyme and substrate concentrations) means comparisons of  $\text{IC}_{50}$  values (often the only reported data) are difficult to interpret. A movement toward reporting inhibition constant ( $\text{K}_i$ ) values, that correct for differences in substrate identity and concentration should be a goal of the field going forward. In this review, reported  $\text{IC}_{50}$  or  $\text{K}_i$  values, where available, will be used to compare reported ATX inhibitors using a relatively coarse scale (where good is  $< 100$  nM, modest is  $< 10$   $\mu\text{M}$ , and poor is more than  $10$   $\mu\text{M}$ ). In addition we have analyzed all ATX inhibitors discussed with respect to Lipinski's 'rule of five' to help predict their likely drug-like potential. Lipinski's 'rule of five' can help predict whether or not new molecules are likely to be orally bioavailable and thus 'drug-like' [54]. Since many ATX inhibitor publications describe a goal to

**Table 1. Unnatural substrates used to study ATX inhibition.** The boxed portion of each substrate is detected upon hydrolysis of the phosphodiester bond by ATX.

Substrate	Detection
 <p data-bbox="533 506 847 539">bis-4-nitrophenylphosphate</p>	Absorbance at 405 nm
 <p data-bbox="416 759 959 792">thymidine 5'-4-nitrophenyl phosphate (pNP-TMP)</p>	Absorbance at 405 nm
 <p data-bbox="628 1173 751 1205">TG-mTMP</p>	<p data-bbox="1235 804 1382 981">Fluorescence system, excitation at 490 nm and emission at 510 nm</p> <p data-bbox="1227 1021 1398 1205">Arrow indicates position of initial ATX cleavage before release of fluorophore.</p>
 <p data-bbox="655 1491 715 1525">CPF4</p>	FRET-based system, excitation at 370 nm and emission at 515 nm
 <p data-bbox="660 1895 710 1926">FS-3</p>	FRET-based system, excitation at 485 nm and emission at 520 nm

create molecules which could potentially be used in a clinical setting, it is important to consider whether or not new inhibitors fit the ‘rule of five’. Compounds matching these rules should have a molecular weight less than 500, not more than 5 H-bond donors, not more than 10 H-bond acceptors, and a calculated Log P (CLogP) less than 5. Inhibitors matching the benchmarks of Lipinski’s rules have a greater chance of solubility and permeability characteristics that make them candidates for oral drug delivery. Veber *et al.* added additional constraints, including a limit of not more than 10 rotatable bonds [55]. Having fewer rotatable bonds reduces the likelihood that the compounds can adopt multiple low-energy conformations and thus have more than one biological target. In the ideal world, potent inhibitors would have one biological target to reduce off-target effects. Both Lipinski’s rules and Veber’s addendum were calculated herein on molecules in ionization states expected at neutral pH using the Molecular Operating Environment (MOE, Chemical Computing Group, Montreal, Canada) for inclusion in all tables that follow.

### Metal chelators as early autotaxin inhibitors

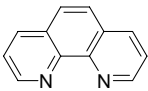
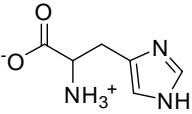
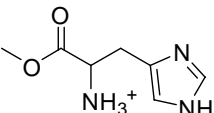
Tokumura *et al.* showed the effect of metal chelators on the activity of an unknown serum metalloenzyme with lysophospholipase-D activity [5]. This work identified the importance of zinc

on the activity of this metalloenzyme—which was later identified as ATX [1, 2]. Indeed, when mouse and rat ATX were first crystallized in 2011, two zinc atoms were present in the nuclease-like domain (Figure 2) [6, 7]. Clair *et al.* was the first to investigate compounds that act as metal chelators to understand the effect of sequestering metal from the active site of ATX [43]. Phenanthroline, histidine, and ethylenediaminetetraacetic acid (EDTA) were tested for ATX inhibition and all three had some effect (Table 2). Both LPC and pNP-TMP were used as substrates to assess ATX inhibition. Although these compounds exhibited no violation to the expanded Lipinski rules (Table 2), potency was poor. In what would become the first structure-activity relationship (SAR) for ATX inhibitors, it was shown that either enantiomer of histidine was the most potent of the compounds tested with the histidine methyl ester being a close second. Imidazole was not an inhibitor of ATX, suggesting that metal chelation alone was not sufficient for inhibition.

### Exploration of lipid-based inhibitors

Shortly after the discovery of ATX inhibition by metal chelators, LPA was discovered to be a feedback inhibitor of ATX [42, 56]. In addition, ATX was also shown to hydrolyze sphingosylphosphorylcholine to generate sphingosine-1-phosphate (S1P), which also acted as a feedback inhibitor of ATX [42, 57].

**Table 2. Select metal chelators with ATX inhibition.** Compound descriptors calculated with MOE include molecular weight (g/mol), number of H-bond donors, number of H-bond acceptors, octanol-water partition coefficient (LogP), and number of rotatable bonds. Potency is described in qualitative terms based on  $IC_{50}$  or  $K_i$  values reported where good is less than 100 nM, modest is less than 10  $\mu$ M, and poor is greater than 10  $\mu$ M.

Name	Structure	Lipinski’s rules				# Rot. bonds	Potency
		Weight	H-don.	H-acc.	LogP		
Phenanthroline [43]		180.21	0	2	2.50	0	Poor
Histidine [43]		155.16	4	3	-1.31	3	Poor
Histidine methyl ester [43]		170.19	4	3	-1.16	4	Poor

It should be noted that Benesch *et al.* later described this inhibition as an artifact of assay conditions, not relevant in presence of physiological amounts of natural substrate (LPC) [56]. Benesch *et al.* showed that LPA and S1P failed to inhibit ATX in the presence of 200  $\mu\text{M}$  LPC, instead of the sub-physiological 1  $\mu\text{M}$  concentration used in the original report. Extensive SAR studies have since been undertaken to explore the SAR and improve the potency of lipid-based ATX inhibitors. Notable compounds to come from these studies are shown in table 3.

Investigations into LPA analogs originally investigated for their activity at the LPA GPCR [58-60], linked ATX inhibition to both cyclic analogs of LPA (such as 2ccPA 16:1, discovered with the FS-3 assay) [61] and non-cyclic lipids (such as BrP-LPA and VPC8a202, using the FS-3 and choline release assays, respectively) [46, 62-65]. Studies of S1P analogs using FS-3 and pNP-TMP as substrates determined FTY720-P was also an ATX inhibitor, in addition to being the bioactive form of FTY720 (an antagonist of S1P<sub>1</sub> signaling used for the treatment of relapsing multiple sclerosis under the trade names GILENYA<sup>®</sup> and fingolimod) [66]. Additional lipids were screened as well, which lead to the identification of a potent lipid inhibitor, S32826 (*via* radiolabeled LPC and choline release assays) [67]. However, S32826 was ineffective *in vivo*—potentially due to hydrolysis of the linking amide bond. Gupte *et al.* developed Gupte 22 and Gupte 30b assayed using FS-3 and pNP-TMP assays (Table 3) [68]. These compounds were predicted to be more effective *in vivo* and solve the potential hydrolytic liability of S32826. Indeed, both Gupte 22 and Gupte 30b showed excellent *in vivo* stability and reduced lung metastases in a syngeneic mouse melanoma model.

During ATX crystallography, Keune *et al.* identified a region of electron density in the hydrophobic tunnel, which lead to the discovery of bound 7- $\alpha$ -hydroxycholesterol (Table 3, Figure 3) [47]. An SAR utilizing commercially available bile salts revealed tauroursodeoxycholic acid (TUDCA, Table 3), and related bile salts as ATX inhibitors. TUDCA was shown to be a noncompetitive inhibitor using choline release

studies, but was a competitive inhibitor when using FS-3 as the substrate. This activity was further explained by crystallographic evidence of TUDCA blocking the open hydrophobic tunnel, which may inhibit LPA release. It is of note that most of these lipid-based inhibitors have modest potency and their flexibility, as reflected by greater than 10 rotatable bonds for all compounds in table 3 other than the steroid derivatives, may predict potential off-target effects.

### Small-molecule, drug-like inhibitors

Until 2008, the most potent ATX inhibitors were lipids. In that year, H2L 7905958 was reported as the first small-molecule, drug-like inhibitor of ATX (Table 4) [69]. Although it has one violation of the Lipinski rules, with a molecular weight slightly above 500 g/mol, H2L 7905958 was the first non-lipid inhibitor of ATX with potency in the low micromolar range, as determined by FS-3, pNP-TMP, and choline release assays [70]. Optimization of this compound showed potency could be improved by installing a trifluoromethyl group into the meta position of the phenylthiourea ring (Hoeglund 11) instead of the initial 3,5-dichloro substitution pattern, although this turned the competitive inhibitor into a non-competitive inhibitor which selectively bound to ATX without effect on catalytic function of NPP6 and NPP7 (lysophospholipid-binding relatives of ATX) [71].

Other groups [39, 72-76], such as Saunders *et al.* [77], also began exploring small-molecule inhibitors to improve on potency, bioavailability, and specificity. During a diversity screen of small molecules, Saunders *et al.* observed inhibition of ATX using both pNP-TMP and FS-3 as substrates. This resulted in the discovery of molecules such as bithionol and NSC 48300 (Table 4). Bithionol showed poor potency and one violation to the expanded Lipinski rules. NSC 48300, on the other hand, was more potent and showed no violations to Lipinski's rules. Inhibition of ATX by these compounds proved to reduce motility and migration of melanoma cells.

During a high-throughput screen, Albers *et al.* identified HA 51 with a combination of substrates including CPF4, bis(*para*-nitrophenyl) phosphate, and LPC. Later, this thiazolidinedione was optimized to HA 155 (potency determined by

**Table 3. Select lipid-based autotaxin inhibitors.** Compound descriptors calculated with MOE include molecular weight (g/mol), number of H-bond donors, number of H-bond acceptors, octanol-water partition coefficient (LogP), and number of rotatable bonds. Potency is described in qualitative terms based on  $IC_{50}$  or  $K_i$  values reported where good is less than 100 nM, modest is less than 10  $\mu$ M, and poor is greater than 10  $\mu$ M.

Name	Structure	Lipinski's rules				# Rot. bonds	Potency
		Weight	H-don.	H-acc.	LogP		
LPA 18:1 [42]		434.51	1	7	4.09	21	Good
2ccPA 16:1 [61]		387.48	0	5	4.06	16	Modest
BrP-LPA [62]		501.40	1	7	5.55	21	Good to modest
VPC8a202 [65]		646.81	2	9	6.38	25	Modest
S1P [42]		378.47	4	5	2.93	17	Good
FTY720-P [66]		386.45	4	5	2.93	14	Modest
S32826 [67]		395.48	1	4	4.88	16	Good
Gupte 22 [68]		380.51	0	3	6.77	16	Modest
Gupte 30b [68]		400.50	0	3	6.95	13	Modest
7- $\alpha$ -hydroxy-cholesterol [47]		402.66	2	2	6.61	5	Not reported
TUDCA [47]		498.71	3	6	3.35	8	Modest

**Table 4. Select small-molecule autotaxin inhibitors.** Compound descriptors calculated with MOE include molecular weight (g/mol), number of H-bond donors, number of H-bond acceptors, octanol-water partition coefficient (LogP), and number of rotatable bonds. Potency is described in qualitative terms based on IC<sub>50</sub> or K<sub>i</sub> values reported where good is less than 100 nM, modest is less than 10 μM, and poor is greater than 10 μM.

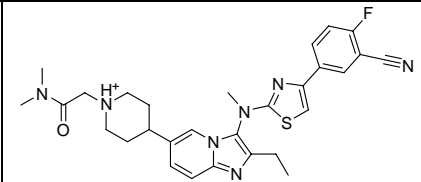
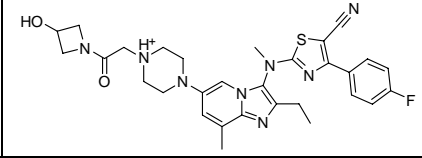
Name	Structure	Lipinski's rules				# Rot. bonds	Potency
		Weight	H-don.	H-acc.	LogP		
H2L 7905958 [69]		506.37	1	5	2.12	6	Modest
Hoeglund 11 [71]		505.50	1	5	1.80	7	Modest
Bithionol [77]		356.06	2	2	6.04	2	Poor
NSC 48300 [77]		412.06	0	6	4.18	4	Modest
HA 51 [50]		474.51	0	6	5.78	8	Modest
HA 155 [78]		463.29	2	5	5.41	7	Good
3BoA [51]		477.20	2	4	5.00	5	Good
Merck B50 [79]		496.42	2	5	2.92	9	Not reported



Table 4 continued..

PF-8380 [49]		479.34	2	5	3.36	8	Good
Merck 19 [80]		518.43	2	5	4.02	7	Modest
Merck 17 [81]		405.34	2	4	5.18	8	Modest
Novartis 35 [82]		440.33	1	5	3.38	9	Modest
Eli Lilly Example 1 [83]		441.50	2	6	0.57	6	Good
918013 [84]		433.29	1	4	2.62	5	Good
403070 [85]		492.22	1	3	4.63	5	Good
PAT-494 [75]		349.37	1	2	3.36	2	Good
PAT-352 [75]		420.42	0	4	3.27	5	Good
PAT-078 [75]		395.41	0	3	6.41	6	Good to modest
PAT-347 [75]		505.93	0	3	6.68	5	Good

Table 4 continued..

Galapagos Compound 171 [86]		546.70	1	4	3.95	9	Good
GLPG-1690 [86]		588.71	2	5	2.16	9	Good

choline release assay, Table 4) by changing the carboxylic acid into a boronic acid which could covalently bind to the nucleophilic threonine in the active site of ATX, although this binding was shown to be reversible [50, 78]. Another group working with boronic acid compounds was able to obtain a potent, non-covalent inhibitor of ATX using a novel substrate of their own design, TG-mTMP. However, they did not compare inhibition of ATX by their compounds, such as 3BoA (Table 4), by using other substrates that are used more pervasively in literature.

Inspired by patented compounds, such as Merck B50 (potency determined by choline release) [79], Pfizer developed PF-8380—one of the most potent ATX inhibitors to date—using FS-3 and LPC with tandem mass spectrometry [49] (Table 4). PF-8380 was shown to reduce LPA levels during inflammation. This small molecule is orally bioavailable, as it proved effective against arthritis upon oral dosing in rats. PF-8380 can be used as a tool to further understand the connection between ATX and inflammatory diseases. Merck has gone on to generate other inhibitors with a scaffold similar to both Merck B50 and PF-8380, such as Merck 19 [80] and Merck 17 [81] (Table 4). Other groups have also synthesized compounds with a polar moiety (such as triazole) and short, hydrophobic tails, as shown in Novartis 35 [82] and Eli Lilly example 1 [83] (Table 4). Merck 17, Novartis 35, and Eli Lilly example 1, all had potency determinations using choline release assays. While the scaffolds were changed slightly in the expanded SAR studies, a recurring theme was dichloro substitution on an aromatic ring. Indeed, this had already been seen with other compounds, such as H2L 7905958.

The availability of crystal structures can allow for structure-based discovery of new scaffolds. Indeed, Fells *et al.* has made use of such structures to understand how small-molecule inhibitors were binding and realized the unique hydrophobic pocket of ATX makes for an allosteric binding site for inhibition by compounds such as 918013 and 403070 (Table 4) as well as others in that SAR series [84, 85]. Potencies for these compounds were determined by a combination of FS-3, pNP-TMP, and choline release assays. Crystallographic techniques have also been applied to ATX complexes with small-molecule inhibitors in order to inform SAR decisions, leading to compounds such as PAT-494, PAT-352, PAT-078, and PAT-347 (Table 4) [75]. Potency for these compounds was determined in a combination of assays including FS-3, bis-NPP, and choline release. Although not available in the Protein Data Bank, Galapagos has shown a crystal structure of GLPG-1690 in presentations, indicating this potent drug compound (as determined by both FS-3 and choline release assays) has been crystallized in ATX, showing occupancy in both the hydrophobic pocket and hydrophobic tunnel [76]. GLPG-1690 was optimized from previous inhibitors, such as compound 171 (Table 4) [86]. It is of note that GPG-1690 is also the only ATX inhibitor currently entering phase II clinical trials [76, 86].

#### Irreversible autotaxin inhibitors

While the field continues to explore reversible small-molecule inhibitors of ATX, other types of inhibitors have also been characterized. Irreversible inhibitors can be useful as a means to understand

the active conformation of the enzyme in addition to being potential treatments for ATX-related diseases. While potency was not reported for Example 3 (Table 5), activity was measured by decreasing hydrolysis of FS-3 [87]. This compound acts as a mechanism-based irreversible inhibitor of ATX, whereupon hydrolysis of the phosphodiester bond produces a reactive quinone methide that can bind to a nucleophile in the active site. Vinyl sulfone compounds, such as CVS-16, are also irreversible inhibitors of ATX activity [88]. These compounds were also analyzed with an FS-3 assay, but dilution assays were also performed to see if the binding was reversible. In fact, the binding of CVS-16 to ATX was irreversible. While CVS-16 showed reduction in tumor volume and serum ATX in melanoma mouse models, PF-8380 did not have a significant impact on melanoma tumor progression when analyzed *via* the same method. When CVS-16 was given at high dosages for an extended period of time, however, dehydration was evident in the mice, and diets were supplemented to combat this side effect. Due to the violations to expanded Lipinski rules, these irreversible inhibitors may not be readily bioavailable and further exploration of this is needed should these types of inhibitors be further developed for clinical use.

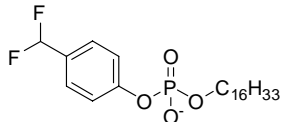
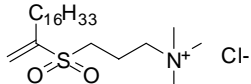
### Structural insights into autotaxin inhibitor binding sites

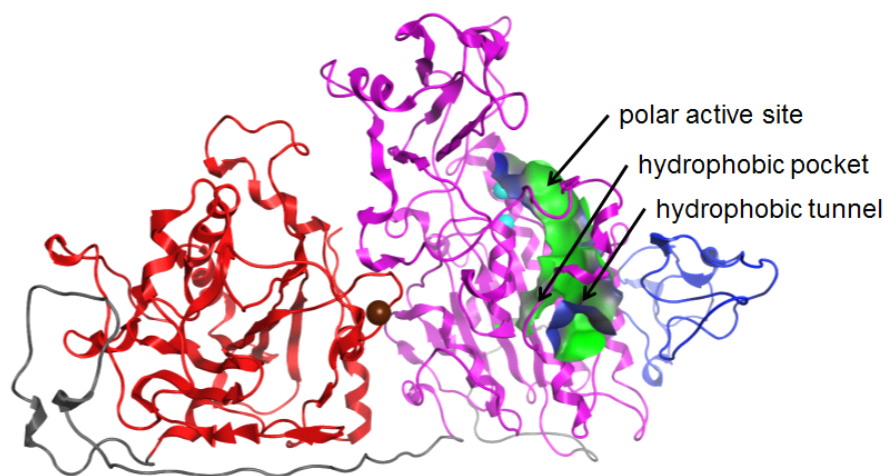
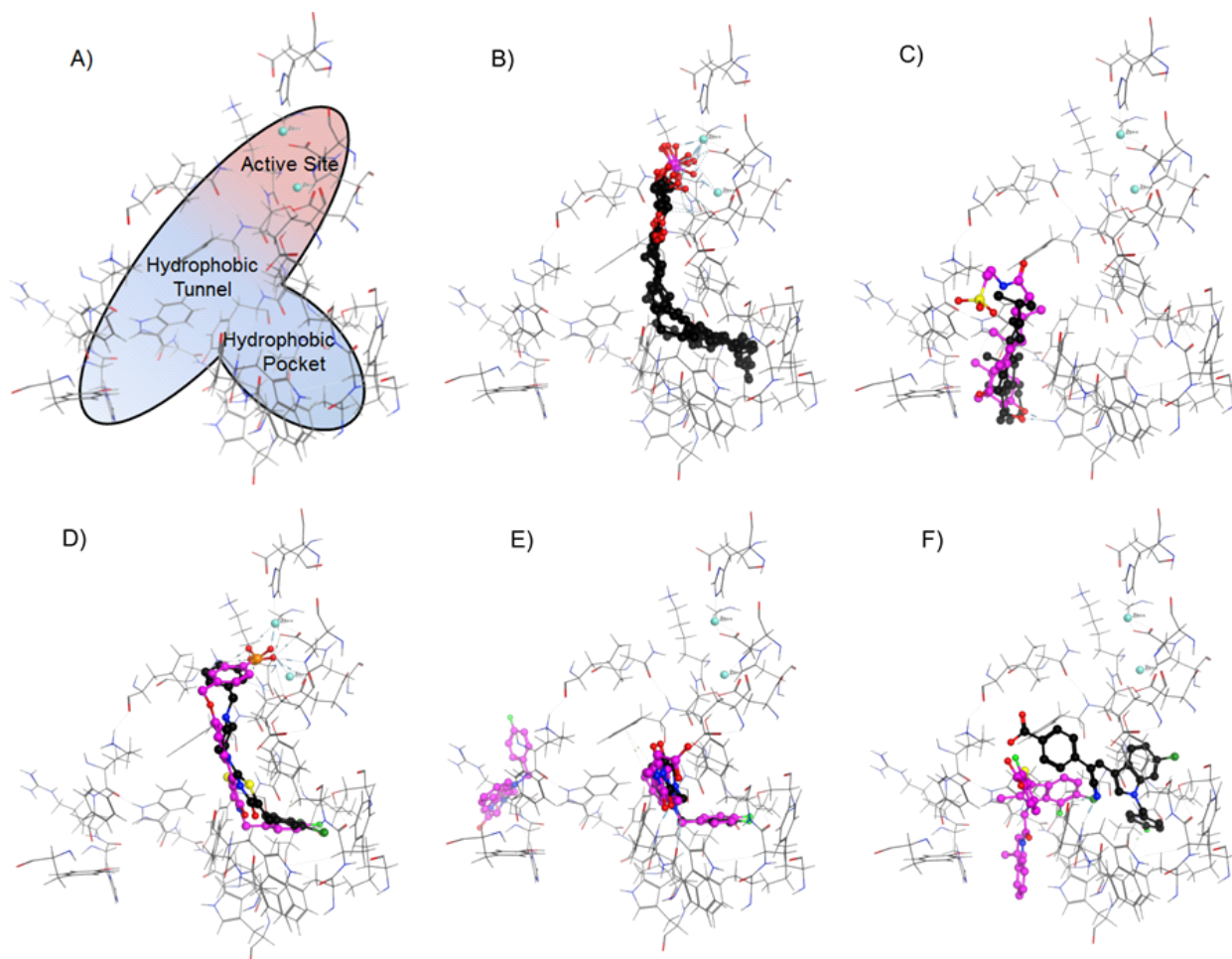
Autotaxin has been crystallized from three different species: mouse (Figure 2), rat, and human [6, 7, 47, 51, 75, 78]. All three show common structural features including a nuclease-like domain,

somatomedin-B-like domains, and a central catalytic domain. Within the catalytic domain, there is an open polar active site, a hydrophobic tunnel, and a hydrophobic pocket. The crystal structures confirmed the presence of zinc and calcium, as theorized by both Tokumura *et al.* and Clair *et al.* during their work with metal chelators as ATX inhibitors [5, 43]. The calcium ion is in the nuclease-like-domain, not the catalytic domain. This could explain why the presence of calcium enhanced ATX activity but could not overcome inhibition caused by histidine [43].

Several crystal structures of ATX in complex with ligands have been published in recent years. Since mouse, rat, and human ATX have high sequence homology (over 95%), the bound structures were aligned to compare inhibitor binding across multiple studies. Figure 3 shows the positions of various co-crystallized compounds superimposed into the catalytic domain of mouse ATX (PDB ID: 3NKM), which were downloaded from the Protein Data Bank [7, 89]. The empty mouse ATX structure is combined with a schematic to more easily visualize the active site, hydrophobic tunnel, and hydrophobic pocket where inhibitors can bind (Figure 3, panel A). One of the first crystal structure papers discussed a series of LPA-bound structures with differing chain lengths (Figure 3, panel B) [7]. The polar head group is shown in complex with the active site and the tail terminates in the hydrophobic pocket. It was theorized that the hydrophobic tunnel was an open exit tunnel for the product. While this may be true, inhibitors that block the tunnel, such as the bile salts discovered by Keune *et al.*, are

**Table 5. Mechanism-based autotaxin inhibitors.** Compound descriptors calculated with MOE include molecular weight (g/mol), number of H-bond donors, number of H-bond acceptors, octanol-water partition coefficient (LogP), and number of rotatable bonds. Potency is described in relative terms of known IC<sub>50</sub> or K<sub>i</sub> values in various assays where good is less than 100 nM, modest is less than 10 μM, and poor is greater than 10 μM.

Name	Structure	Lipinski's rules				# Rot. bonds	Potency
		Weight	H-don.	H-acc.	LogP		
University of Memphis Example 3 [87]		447.52	0	2	8.04	19	Not reported
CVS-16 [88]		416.74	0	2	7.02	20	Modest

**Figure 2****Figure 3**

non-competitive inhibitors of LPC hydrolysis, although they do show competitive inhibition for FS-3 hydrolysis (Figure 3, panel C) [47].

Small molecules have also been crystallized in complex with ATX by multiple groups. The reversible covalent binding of HA155 to the catalytic threonine was explained by Hausmann *et al.* using one of the first ATX complexes with a small-molecule inhibitor [6]. The crystal structure of HA155 contained a tetrahedral boron, which is indicative of forming a covalent bond with the catalytic threonine. Albers *et al.* showed this covalent bond was reversible by utilizing a washout assay [45]. Kawaguchi *et al.* published ATX complexes with other boronic acid inhibitors, like 3BoA, in which boron has a trigonal planar geometry, indicating a non-covalent interaction with the polar active site [51]. Modeling-based discovery of novel inhibitors of ATX may need to include water in the simulations because, as mentioned by Kawaguchi *et al.*, ATX may interact with some inhibitors *via* a bridging water molecule. Both boronic acid analogs were shown to interact with the polar active site and terminate in the hydrophobic pocket (Figure 3, panel D). In the first crystal structure of human ATX, Stein *et al.* provide further evidence supporting the importance of evaluating inhibitors using multiple substrates as analogous compounds can bind in different areas of the catalytic domain [75]. They coupled the crystallographic data with mechanistic determinations for each compound. PAT-352,

which is analogous to PAT-494 (Table 4), is shown in two locations within the catalytic domain—one in the hydrophobic tunnel and one in the hydrophobic pocket (PDB ID: 4ZG9, Figure 3, panel E). PAT-494, the smaller analog, is also shown in the hydrophobic pocket (PDB ID: 4ZGA, Figure 3, panel E). Both of these compounds are mixed mode-inhibitors of choline release from LPC, but only PAT-352 shows inhibition with FS-3. The other two potent inhibitors studied by Stein *et al.* are PAT-078 and the analogous compound, PAT-347 (Table 4). As seen in the crystal structures (Figure 3, panel F), PAT-078 is in the hydrophobic pocket of ATX while PAT-347 occupies the hydrophobic tunnel. These binding differences can explain why PAT-078 is a competitive inhibitor, showing residency in the hydrophobic pocket which would typically be occupied by the lipophilic tail of the natural substrate, LPC. Meanwhile, PAT-347 is a non-competitive inhibitor, much like the bile salts, occupying the hydrophobic tunnel. Even though compounds are analogous to one another, the binding position differences displayed in these crystal structures demonstrate that they may not occupy the same binding site, the ATX catalytic domain. As more small molecules are developed for ATX inhibition, crystal structures such as these can be used as a tool to understand binding and how it relates to inhibitory activity of novel compounds.

Although computational modeling identified the first non-lipid inhibitors of ATX using a model

---

**Legend to Figure 2.** A Representative ATX Crystal Structure (PDB ID: 3NKM). The two N-terminal somatomedin-B-like domains are shown as a blue ribbon. The catalytic domain is shown as a pink ribbon with the surface around the binding site rendered with hydrophobic surfaces in green and hydrophilic surfaces in blue. Two zinc ions (aqua spheres) are in the active site. A calcium ion (brown sphere) is in the nuclease-like-domain (red ribbon). Two linker regions are shown as a dark gray ribbon.

**Legend to Figure 3.** Crystallographic positions of known ATX inhibitors as superposed in mouse ATX (mATX) (PDB ID: 3NKM). Panel A shows the empty active site of mATX with a cartoon indicating the locations of the polar active site, the hydrophobic tunnel, and the hydrophobic pocket [7, 89]. Panel B shows the structures of crystallized LPA extending from the active site down into the hydrophobic pocket (PDB ID: 3NKN, 3NKO, 3NKP, 3NKQ, and 3NKR) [7, 89]. Panel C displays both 7- $\alpha$ -hydroxycholesterol (fuschia, table 3, PDB ID: 5DLT) and TUDCA (black, table 3, PDB ID: 5DLV) [47, 89]. Panel D shows the locations of 3BoA (black, table 4, PDB ID: 3WAX, [51]) and HA 155 (fuschia, table 4, PDB ID: 2XRG [6]) [89]. Panel E shows two possible binding locations of PAT-352 (fuschia, table 4, PDB ID: 4ZG9) and one crystallized location of PAT-494 (black, table 4, PDB ID: 4ZGA) [75, 89]. Panel F displays different binding locales of inhibitor analogs PAT-078 (black, table 4, PDB ID: 4ZG6) and PAT-347 (fuschia, table 4, PDB ID: 4ZG7) [75, 89].

that only included the catalytic domain [69], the crystallographic ATX structures provide more complete starting points for structure-based discovery of novel inhibitors. This has been done by multiple groups, including Fells *et al.* in the discovery of small-molecule inhibitors of ATX and optimization of those inhibitors to obtain 918013 and 403070, as well as other compounds (Table 4) [84, 85]. Modeling and crystallographic evidence, both point to the hydrophobic pocket as an important area for ATX inhibition, as seen in figure 3, panels D, E, and F. Further development of computational models that use existing crystallographic data will discover new inhibitors in the future.

### CONCLUDING REMARKS

The connection of ATX to various disease states has led to an increased interest in studying inhibition. These studies have informed the field in how molecules interact with ATX, leading to compounds that can potentially be used as leads toward treatment strategies for ATX-related diseases. The most potent inhibitors to date have an overall amphipathic quality with a polar group and relatively non-polar, aromatic substituents. S32826, the most potent lipid-based inhibitor, contains a phosphonate head group connected to an *N*-phenylactylamide (Table 3). PF-8380, the most potent small-molecule inhibitor, has a substituted benzo[*d*]oxazol-2(3*H*)-one head group and a 3,5-dichlorobenzyl moiety (Table 4). However, PAT-352, PAT-078, and PAT-347 have a carboxylate with various aromatic substituents (Table 4). Reduction of flexibility by making use of ring systems instead of long, lipid tails has also led to compounds with increased specificity, which can translate into fewer side effects when used as pharmaceutical agents. For instance, LPA and S1P (Table 3) act as ATX inhibitors and agonists for GPCR signaling [15-17, 42, 57], whereas Hoeglund 11 (Table 4) has markedly fewer rotatable bonds and has been shown to be selective for ATX over lipid-binding family members NPP6 and NPP7 [71]. Additionally, GLPG-1690 was developed with reduced flexibility and basicity, making use of crystal structures and activity assays [76]. Optimizing the piperazine ring on GLPG-1690 allowed for reduced inhibition

of hERG (human Ether-a-go-go-Related Gene), which is associated with sudden death. With the plethora of crystallographic data available, the field will continue to expand the discovery and optimization of new inhibitors by using existing crystal structures for structure-based modeling or by solving structures of inhibitors in complex with ATX. Continued structure-activity relationship studies will explore new scaffolds to find differing mechanisms of binding to ATX which can be useful to further understand the activity of this ubiquitous enzyme. There is a relatively high attrition rate when converting hit compounds into approved drugs, as described by both Hughes *et al.* and Borchardt [90, 91]. In Alzheimer's disease, for instance, the attrition rate for compounds moving through clinical trials increased with each phase [92]. Over a decade, only 0.4% of Alzheimer's drugs entering clinical trials gained regulatory approval after Phase 3. Failure rates may vary substantially in different diseases, but having more than just a relatively small number of potent, drug-like compounds will increase the chances of future conversion of ATX inhibitors into clinically-useful drugs.

Currently, GLPG-1690 is the only ATX inhibitor in clinical trials (Table 4, for idiopathic pulmonary fibrosis). However, there are several other scaffolds available with nanomolar potencies. These scaffolds could be investigated in cytotoxicity assays and mouse models to analyze pharmacokinetics and pharmacodynamics before moving into the clinical setting as potential treatments for other ATX-related diseases. An analog of S32826 was injected into ATX-heterozygous mice to treat allergic asthma, reducing plasma LPA levels and decreasing lung inflammation [35]. This demonstrates ATX could be a viable target for the treatment of severe asthma. ATX inhibitors could also be examined in coronary artery syndrome, where it has been shown that patients have significantly higher concentrations of ATX [33]. Inhibition of ATX activity could also be a potential treatment for Alzheimer-type dementia [37]. The field has been focused on cancer research, as ATX was initially identified from melanoma cells. However, the field would benefit from analyzing potent inhibitors in systems to target other ATX-related diseases as well.

## ACKNOWLEDGEMENTS

Thanks to the Chemical Computing Group, Montreal, Canada for the Molecular Operating Environment (MOE).

## CONFLICT OF INTEREST STATEMENT

The authors confirm that this article content has no conflicts of interest.

## REFERENCES

1. Tokumura, A., Majima, E., Kariya, Y., Tominaga, K., Kogure, K., Yasuda, K. and Fukuzawa, K. 2002, *J. Biol. Chem.*, 277, 39436-42.
2. Umezu-Goto, M., Kishi, Y., Taira, A., Hama, K., Dohmae, N., Takio, K., Yamori, T., Mills, G. B., Inoue, K., Aoki, J. and Arai, H. 2002, *J. Cell Biol.*, 158, 227-33.
3. Yamashita, M., Homma, H., Inoue, K. and Nojima, S. 1983, *J. Toxicol. Sci.*, 8, 177-88.
4. Tokumura, A., Harada, K., Fukuzawa, K. and Tsukatani, H. 1986, *Biochim. Biophys. Acta*, 875, 31-8.
5. Tokumura, A., Miyake, M., Yoshimoto, O., Shimizu, M. and Fukuzawa, K. 1998, *Lipids*, 33, 1009-15.
6. Hausmann, J., Kamtekar, S., Christodoulou, E., Day, J. E., Wu, T., Fulkerson, Z., Albers, H. M., van Meeteren, L. A., Houben, A. J., van Zeijl, L., Jansen, S., Andries, M., Hall, T., Pegg, L. E., Benson, T. E., Kasiem, M., Harlos, K., Kooi, C. W., Smyth, S. S., Ovaa, H., Bollen, M., Morris, A. J., Moolenaar, W. H. and Perrakis, A. 2011, *Nat. Struct. Mol. Biol.*, 18, 198-204.
7. Nishimasu, H., Okudaira, S., Hama, K., Mihara, E., Dohmae, N., Inoue, A., Ishitani, R., Takagi, J., Aoki, J. and Nureki, O. 2011, *Nat. Struct. Mol. Biol.*, 18, 205-12.
8. Stracke, M. L., Krutzsch, H. C., Unsworth, E. J., Arestad, A., Cioce, V., Schiffmann, E. and Liotta, L. A. 1992, *J. Biol. Chem.*, 267, 2524-9.
9. Clair, T., Lee, H. Y., Liotta, L. A. and Stracke, M. L. 1997, *J. Biol. Chem.*, 272, 996-1001.
10. Jansen, S., Stefan, C., Creemers, J. W., Waelkens, E., van Eynde, A., Stalmans, W. and Bollen, M. 2005, *J. Cell. Sci.*, 118, 3081-9.
11. Bollen, M., Gijssbers, R., Ceulemans, H., Stalmans, W. and Stefan, C. 2000, *Crit. Rev. Biochem. Mol. Biol.*, 35, 393-432.
12. Albright, R. A., Ornstein, D. L., Cao, W., Chang, W. C., Robert, D., Tehan, M., Hoyer, D., Liu, L., Stabach, P., Yang, G., De La Cruz, E. M. and Braddock, D. T. 2014, *J. Biol. Chem.*, 289, 3294-306.
13. Albright, R. A., Chang, W. C., Robert, D., Ornstein, D. L., Cao, W., Liu, L., Redick, M. E., Young, J. I., De La Cruz, E. M. and Braddock, D. T. 2012, *Blood*, 120, 4432-40.
14. Stefan, C., Jansen, S. and Bollen, M. 2005, *Trends Biochem. Sci.*, 30, 542-50.
15. Moolenaar, W. H. 2002, *The Journal of Cell Biology*, 158, 197-9.
16. Luquain, C., Sciorra, V. A. and Morris, A. J. 2003, *Trends Biochem. Sci.*, 28, 377-83.
17. Panupinthu, N., Lee, H. Y. and Mills, G. B. 2010, *Br. J. Cancer*, 102, 941-6.
18. Stam, J. C., Michiels, F., van der Kammen, R. A., Moolenaar, W. H. and Collard, J. G. 1998, *EMBO J.*, 17, 4066-74.
19. Tokumura, A., Kanaya, Y., Miyake, M., Yamano, S., Irahara, M. and Fukuzawa, K. 2002, *Biol. Reprod.*, 67, 1386-92.
20. Tanaka, M., Okudaira, S., Kishi, Y., Ohkawa, R., Iseki, S., Ota, M., Noji, S., Yatomi, Y., Aoki, J. and Arai, H. 2006, *J. Biol. Chem.*, 281, 25822-30.
21. van Meeteren, L. A., Ruurs, P., Stortelers, C., Bouwman, P., van Rooijen, M. A., Pradere, J. P., Pettit, T. R., Wakelam, M. J., Saulnier-Blache, J. S., Mummery, C. L., Moolenaar, W. H. and Jonkers, J. 2006, *Mol. Cell. Biol.*, 26, 5015-22.
22. Benesch, M. G., Ko, Y. M., McMullen, T. P. and Brindley, D. N. 2014, *FEBS Lett.*, 588, 2712-27.
23. St-Coeur, P. D., Ferguson, D., Morin, P. Jr. and Touaibia, M. 2013, *Arch. Pharm. (Weinheim)*, 346, 91-7.
24. Hoelzinger, D. B., Nakada, M., Demuth, T., Rosensteel, T., Reavie, L. B. and Berens, M. E. 2008, *J. Neurooncol.*, 86, 297-309.
25. Ortlepp, C., Steudel, C., Heiderich, C., Koch, S., Jacobi, A., Ryser, M., Brenner, S., Bornhauser, M., Brors, B., Hofmann, W. K., Ehninger, G. and Thiede, C. 2013, *Exp. Hematol.*, 41, 444-461.e4.

26. Benesch, M. G., Tang, X., Dewald, J., Dong, W. F., Mackey, J. R., Hemmings, D. G., McMullen, T. P. and Brindley, D. N. 2015, *FASEB J.*, 29, 3990-4000.
27. Benesch, M. G., Ko, Y. M., Tang, X., Dewald, J., Lopez-Campistrous, A., Zhao, Y. Y., Lai, R., Curtis, J. M., Brindley, D. N. and McMullen, T. P. 2015, *Endocr. Relat. Cancer*, 22, 593-607.
28. Su, S. C., Hu, X., Kenney, P. A., Merrill, M. M., Babaian, K. N., Zhang, X. Y., Maity, T., Yang, S. F., Lin, X. and Wood, C. G. 2013, *Clin. Cancer Res.*, 19, 6461-72.
29. Vidot, S., Witham, J., Agarwal, R., Greenhough, S., Bamrah, H. S., Tigyi, G. J., Kaye, S. B. and Richardson, A. 2010, *Cell. Signal.*, 22, 926-35.
30. Samadi, N., Bekele, R. T., Goping, I. S., Schang, L. M. and Brindley, D. N. 2011, *PLoS One*, 6, e20608.
31. El-Batch, M., Ibrahim, W. and Said, S. 2011, *J. Biochem. Mol. Toxicol.*, 25, 143-50.
32. Tager, A. M. 2012, *Am. J. Respir. Cell Mol. Biol.*, 47, 563-5.
33. Dohi, T., Miyauchi, K., Ohkawa, R., Nakamura, K., Kishimoto, T., Miyazaki, T., Nishino, A., Nakajima, N., Yaginuma, K., Tamura, H., Kojima, T., Yokoyama, K., Kurata, T., Shimada, K., Yatomi, Y. and Daida, H. 2012, *Clinica Chimica Acta*, 413, 207-12.
34. Inoue, M., Rashid, M. H., Fujita, R., Contos, J. J., Chun, J. and Ueda, H. 2004, *Nat. Med.*, 10, 712-8.
35. Park, G. Y., Lee, Y. G., Berdyshev, E., Nyenhuis, S., Du, J., Fu, P., Gorshkova, I. A., Li, Y., Chung, S., Karpurapu, M., Deng, J., Ranjan, R., Xiao, L., Jaffe, H. A., Corbridge, S. J., Kelly, E. A., Jarjour, N. N., Chun, J., Prestwich, G. D., Kaffe, E., Ninou, I., Aidinis, V., Morris, A. J., Smyth, S. S., Ackerman, S. J., Natarajan, V. and Christman, J. W. 2013, *Am. J. Respir. Crit. Care Med.*, 188, 928-40.
36. Velasco, M., O'Sullivan, C. and Sheridan, G. K. 2016, *Neuropharmacology*, pii: S0028-3908(16)30129-0.
37. Umemura, K., Yamashita, N., Yu, X., Arima, K., Asada, T., Makifuchi, T., Murayama, S., Saito, Y., Kanamaru, K., Goto, Y., Kohsaka, S., Kanazawa, I. and Kimura, H. 2006, *Neurosci. Lett.*, 400, 97-100.
38. Rancoule, C., Dusaulcy, R., Treguer, K., Gres, S., Attane, C. and Saulnier-Blache, J. S. 2014, *Biochimie.*, 96, 140-3.
39. Albers, H. M., Dong, A., van Meeteren, L. A., Egan, D. A., Sunkara, M., van Tilburg, E. W., Schuurman, K., van Tellingen, O., Morris, A. J., Smyth, S. S., Moolenaar, W. H. and Ovaa, H. 2010, *Proc. Natl. Acad. Sci. USA*, 107, 7257-62.
40. Murph, M., Tanaka, T., Pang, J., Felix, E., Liu, S., Trost, R., Godwin, A. K., Newman, R. and Mills, G. 2007, *Methods Enzymol.*, 433, 1-25.
41. Scherer, M., Schmitz, G. and Liebisch, G. 2009, *Clin. Chem.*, 55, 1218-22.
42. van Meeteren, L. A., Ruurs, P., Christodoulou, E., Goding, J. W., Takakusa, H., Kikuchi, K., Perrakis, A., Nagano, T. and Moolenaar, W. H. 2005, *J. Biol. Chem.*, 280, 21155-61.
43. Clair, T., Koh, E., Ptaszynska, M., Bandle, R. W., Liotta, L. A., Schiffmann, E. and Stracke, M. L. 2005, *Lipids Health Dis.*, 4, 5.
44. Hoeglund, A. B., Howard, A. L., Wanjala, I. W., Pham, T. C., Parrill, A. L. and Baker, D. L. 2010, *Bioorg. Med. Chem.*, 18, 769-76.
45. Albers, H. M., van Meeteren, L. A., Egan, D. A., van Tilburg, E. W., Moolenaar, W. H. and Ovaa, H. 2010, *J. Med. Chem.*, 53, 4958-67.
46. Nikitopoulou, I., Kaffe, E., Sevastou, I., Sirioti, I., Samiotaki, M., Madan, D., Prestwich, G. D. and Aidinis, V. 2013, *PLoS One*, 8, e70941. doi:10.1371/journal.pone.0070941.
47. Keune, W. J., Hausmann, J., Bolier, R., Tolenaars, D., Kremer, A., Heidebrecht, T., Joosten, R. P., Sunkara, M., Morris, A. J., Matas-Rico, E., Moolenaar, W. H., Oude Elferink, R. P. and Perrakis, A. 2016, *Nat. Commun.*, 7, 11248.
48. Albers, H. M., Hendrickx, L. J., van Tol, R. J., Hausmann, J., Perrakis, A. and Ovaa, H. 2011, *J. Med. Chem.*, 54, 4619-26.
49. Gierse, J., Thorarensen, A., Beltey, K., Bradshaw-Pierce, E., Cortes-Burgos, L., Hall, T., Johnston, A., Murphy, M.,



- Nemirovskiy, O., Ogawa, S., Pegg, L., Pelc, M., Prinsen, M., Schnute, M., Wendling, J., Wene, S., Weinberg, R., Wittwer, A., Zweifel, B. and Masferrer, J. 2010, *J. Pharmacol. Exp. Ther.*, 334, 310-7.
50. Albers, H. M., van Meeteren, L. A., Egan, D. A., van Tilburg, E. W., Moolenaar, W. H. and Ovaa, H. 2010, *J. Med. Chem.*, 53, 4958-67.
51. Kawaguchi, M., Okabe, T., Okudaira, S., Nishimasu, H., Ishitani, R., Kojima, H., Nureki, O., Aoki, J. and Nagano, T. 2013, *ACS Chem. Biol.*, 8, 1713-21.
52. Takakusa, H., Kikuchi, K., Urano, Y., Sakamoto, S., Yamaguchi, K. and Nagano, T. 2002, *J. Am. Chem. Soc.*, 124, 1653-7.
53. Ferguson, C. G., Bigman, C. S., Richardson, R. D., van Meeteren, L. A., Moolenaar, W. H. and Prestwich, G. D. 2006, *Org. Lett.*, 8, 2023-6.
54. Lipinski, C. A., Lombardo, F., Dominy, B. W. and Feeney, P. J. 2001, *Adv. Drug Deliv. Rev.*, 46, 3-26.
55. Veber, D. F., Johnson, S. R., Cheng, H. Y., Smith, B. R., Ward, K. W. and Kopple, K. D. 2002, *J. Med. Chem.*, 45, 2615-23.
56. Benesch, M. G., Zhao, Y. Y., Curtis, J. M., McMullen, T. P. and Brindley, D. N. 2015, *J. Lipid Res.*, 56, 1134-44.
57. Clair, T., Aoki, J., Koh, E., Bandle, R. W., Nam, S. W., Ptaszynska, M. M., Mills, G. B., Schiffmann, E., Liotta, L. A. and Stracke, M. L. 2003, *Cancer Res.*, 63, 5446-53.
58. Fischer, D. J., Liliom, K., Guo, Z., Nusser, N., Virag, T., Murakami-Murofushi, K., Kobayashi, S., Erickson, J. R., Sun, G., Miller, D. D. and Tigyi, G. 1998, *Mol. Pharmacol.*, 54, 979-88.
59. Jiang, G., Xu, Y., Fujiwara, Y., Tsukahara, T., Tsukahara, R., Gajewiak, J., Tigyi, G. and Prestwich, G. D. 2007, *ChemMedChem.*, 2, 679-90.
60. Heasley, B. H., Jarosz, R., Carter, K. M., van, S. J., Lynch, K. R. and Macdonald, T. L. 2004, *Bioorg. Med. Chem. Lett.*, 14, 4069-74.
61. Baker, D. L., Fujiwara, Y., Pigg, K. R., Tsukahara, R., Kobayashi, S., Murofushi, H., Uchiyama, A., Murakami-Murofushi, K., Koh, E., Bandle, R. W., Byun, H. S., Bittman, R., Fan, D., Murph, M., Mills, G. B. and Tigyi, G. 2006, *J. Biol. Chem.*, 281, 22786-93.
62. Zhang, H., Xu, X., Gajewiak, J., Tsukahara, R., Fujiwara, Y., Liu, J., Fells, J. I., Perygin, D., Parrill, A. L., Tigyi, G. and Prestwich, G. D. 2009, *Cancer Res.*, 69, 5441-9.
63. Cui, P., Tomsig, J. L., McCalmont, W. F., Lee, S., Becker, C. J., Lynch, K. R. and Macdonald, T. L. 2007, *Bioorg. Med. Chem. Lett.*, 17, 1634-40.
64. Cui, P., McCalmont, W. F., Tomsig, J. L., Lynch, K. R. and Macdonald, T. L. 2008, *Bioorg. Med. Chem.*, 16, 2212-25.
65. East, J. E., Kennedy, A. J., Tomsig, J. L., De Leon, A. R., Lynch, K. R. and Macdonald, T. L. 2010, *Bioorg. Med. Chem. Lett.*, 20, 7132-6.
66. van Meeteren, L. A., Brinkmann, V., Saulnier-Blache, J., Lynch, K. R. and Moolenaar, W. H. 2008, *Cancer Lett.*, 266, 203-8.
67. Ferry, G., Moulharat, N., Pradere, J. P., Desos, P., Try, A., Genton, A., Giganti, A., Beucher-Gaudin, M., Lonchamp, M., Bertrand, M., Saulnier-Blache, J. S., Tucker, G. C., Cordi, A. and Boutin, J. A. 2008, *J. Pharmacol. Exp. Ther.*, 327, 809-19.
68. Gupte, R., Patil, R., Liu, J., Wang, Y., Lee, S. C., Fujiwara, Y., Fells, J., Bolen, A. L., Emmons-Thompson, K., Yates, C. R., Siddam, A., Panupinthu, N., Pham, T. T., Baker, D. L., Parrill, A. L., Mills, G. B., Tigyi, G. and Miller, D. D. 2011, *ChemMedChem.*, 6, 922-35.
69. Parrill, A. L., Echols, U., Nguyen, T., Pham, T. C., Hoeglund, A. and Baker, D. L. 2008, *Bioorg. Med. Chem.*, 16, 1784-95.
70. Hoeglund, A. B., Howard, A. L., Wanjala, I. W., Pham, T. C., Parrill, A. L. and Baker, D. L. 2010, *Bioorg. Med. Chem.*, 18, 769-76.
71. Hoeglund, A. B., Bostic, H. E., Howard, A. L., Wanjala, I. W., Best, M. D., Baker, D. L. and Parrill, A. L. 2010, *J. Med. Chem.*, 53, 1056-66.
72. Gierse, J., Thorarensen, A., Beltey, K., Bradshaw-Pierce, E., Cortes-Burgos, L., Hall, T., Johnston, A., Murphy, M., Nemirovskiy, O.,

- Ogawa, S., Pegg, L., Pelc, M., Prinsen, M., Schnute, M., Wendling, J., Wene, S., Weinberg, R., Wittwer, A., Zweifel, B. and Masferrer, J. 2010, *J. Pharmacol. Exp. Ther.*, 334, 310-7.
73. North, E. J., Howard, A. L., Wanjala, I. W., Pham, T. C., Baker, D. L. and Parrill, A. L. 2010, *J. Med. Chem.*, 53, 3095-105.
74. Ragle, L. E., Palanisamy, D. J., Joe, M. J., Stein, R. S., Norman, D. D., Tigyi, G., Baker, D. L. and Parrill, A. L. 2016, *Bioorg. Med. Chem.*, 24, 4660-74.
75. Stein, A. J., Bain, G., Prodanovich, P., Santini, A. M., Darlington, J., Stelzer, N. M., Sidhu, R. S., Schaub, J., Goulet, L., Lonergan, D., Calderon, I., Evans, J. F. and Hutchinson, J. H. 2015, *Mol. Pharmacol.*, 88, 982-92.
76. Desroy, N. 2016, Discovery of GLPG1690: A first-in-class autotaxin inhibitor in clinical development for the treatment of idiopathic pulmonary fibrosis. <http://www.glpg.com/docs/view/570b896b91744-en>
77. Saunders, L. P., Ouellette, A., Bandle, R., Chang, W. C., Zhou, H., Misra, R. N., De La Cruz, E. M. and Braddock, D. T. 2008, *Mol. Cancer Ther.*, 7, 3352-62.
78. Albers, H. M., Hendrickx, L. J., van Tol, R. J., Hausmann, J., Perrakis, A. and Ovaa, H. 2011, *J. Med. Chem.*, 54, 4619-26.
79. Schiemann, K., Schultz, M., Blaukat, A. and Kober, I. 2009, Patent No. WO2009046841A2.
80. Schiemann, K., Schultz, M. and Staehle, W. 2010, Patent No. WO2010115491A2.
81. Staehle, W., Schiemann, K. and Schultz, M. 2010, Patent No. WO2010112116A1.
82. Furminger, V., Hughes, O. R., Legrand, D. M., Stanley, E. and Thomson, C. 2014, Patent No. US20140171404A1.
83. Bleisch, T. J., Doti, R. A., Pfeifer, L. A. and Norman, B. H. 2014, Patent No. WO2014168824A1.
84. Fells, J. I., Lee, S. C., Fujiwara, Y., Norman, D. D., Lim, K. G., Tsukahara, R., Liu, J., Patil, R., Miller, D. D., Kirby, R. J., Nelson, S., Seibel, W., Papoian, R., Parrill, A. L., Baker, D. L., Bittman, R. and Tigyi, G. 2013, *Mol. Pharmacol.*, 84, 415-24.
85. Fells, J. I., Lee, S. C., Norman, D. D., Tsukahara, R., Kirby, J. R., Nelson, S., Seibel, W., Papoian, R., Patil, R., Miller, D. D., Parrill, A. L., Pham, T. C., Baker, D. L., Bittman, R. and Tigyi, G. 2014, *FEBS J.*, 281, 1017-28.
86. Desroy, N., Heckmann, B., Brys, R. C. X., Joncour, A., Peixoto, C. and Bock, X. 2014, Patent No. WO2014139882A1.
87. Parrill-Baker, A., Baker, D. L. and Montedonico, L. E. 2010, Patent No. WO2010040080A1.
88. Murph, M. M., Jiang, G. W., Altman, M. K., Jia, W., Nguyen, D. T., Fambrough, J. M., Hardman, W. J., Nguyen, H. T., Tran, S. K., Alshamrani, A. A., Madan, D., Zhang, J. and Prestwich, G. D. 2015, *Bioorg. Med. Chem.*, 23, 5999-6013.
89. Berman, H. M., Westbrook, J., Feng, Z., Gilliland, G., Bhat, T. N., Weissig, H., Shindyalov, I. N. and Bourne, P. E. 2000, *Nucleic Acids Res.*, 28, 235-42.
90. Hughes, J., Rees, S., Kalindjian, S. and Philpott, K. 2011, *Br. J. Pharmacol.*, 162, 1239-49.
91. Borchardt, R. 2004, *Pharmaceutical Profiling in Drug Discovery for Lead Selection*. R. Borchardt, E. Kerns, C. Lipinski, D. Thakker and W. Binghe (Eds.), 451-466. Arlington, VA: AAPS Press.
92. Cummings, J. L., Morstorf, T. and Zhong, K. 2014, *Alzheimers Res. Ther.*, 6, 37.